Frictional properties of chain alcohols and the dynamics of layering transitions

Frieder Mugele[1, 2, *] Bo Persson[3], Silviu Zilberman[4], Abraham Nitzan[4], and Miquel Salmeron[2]

[1] *Universität Ulm; Abteilung Angewandte Physik; Albert Einstein Allee 11; D-89081 Ulm (Germany)*
[2] *Materials Science Department; Lawrence Berkeley National Laboratory; Berkeley, CA 94720 (USA)*
[3] *Institut für Festkörperforschung, Forschungszentrum Jülich, D-52425 Jülich (Germany)*
[4] *School of Chemistry, Tel Aviv University, Tel-Aviv 69978 (Israel)*

We used a Surface Forces Apparatus to investigate layering transitions and frictional properties of chain alcohol films. All but the last two monolayers, strongly bound to each mica surface can be removed by squeezing. Unlike other systems however, chain alcohol films of undecanol and octanol were found to retain their bulk-like lubrication properties down to a thickness of only one (bi)layer. The transition where this last molecularly thin liquid layer is expelled from the gap proceeds in less than one second. From two-dimensional snapshots of the contact area during the expulsion process, we find that the boundary line between the areas of initial and final film thickness bends and roughens as it moves across the contact area. In the final state, we frequently find pockets of trapped liquid. Both the bending and roughening of the boundary line and the trapped pockets are due to a dynamic instability that we describe with a two-dimensional hydrodynamic model. The length scale of the roughening is determined by an elastic line tension.

* Author to whom correspondence should be addressed. Electronic mail: frieder.mugele@physik.uni-ulm.de

Introduction

The arrangement of liquid molecules near a solid surface differs from the bulk structure. On sufficiently smooth interfaces, the liquid molecules form a layered structure as shown experimental and theoretical for systems ranging from rare gas atoms [1, 2] over metals [3] to organic liquids [4]. The range of this layered structure is typically a few atomic or molecular diameters, depending on the specific system. In the case of a pore, where two solid surfaces face each other at a small distance, the whole liquid film can be restructured. In a surface forces apparatus (SFA), this leads to a series of so-called layering transitions as the two atomically smooth mica surfaces are pressed together continuously. Each time the normal force exceeds certain critical values the film thickness decreases abruptly by an amount that is related to the dimension of the liquid particles [4]. Frequently it has been reported that the structural modifications lead to dramatically different mechanical properties. For instance, a sudden appearance of solid-like stick-slip friction was found in SFA experiments [5, 6] when the thickness of various films was less than 4 to 6 molecular layers. The frictional properties of these films are also of crucial importance to the dynamics of layering transitions. For liquid-like layers, a layering transition can be described as a hydrodynamic process, whereas solid-like layers can only "flow" by either plastic deformation, brittle fracture, or after some (e.g. stress-induced) transition to the liquid state.

Here, we present experiments with chain alcohols, namely octanol (C_8OH) and undecanol ($C_{11}OH$), confined between atomically smooth mica surfaces in a SFA. The OH-group of these molecules introduces a strong anisotropy to the interaction both between the liquid molecules and the substrate and amongst the liquid molecules themselves. This leads to the formation of self-assembled monolayers strongly bound to each surface, and a complicated bilayer structure in the additional liquid. A combination of optical sum frequency generation and SFA force-distance measurements was used to determine a structural model for the alcohol films that is summarized in Fig. 1 [7]. While the bound monolayers are inert and effectively part of the substrate, the average polar tilt angle of the molecules in the bilayers increases continuously as the surfaces are pressed together. At critical average tilt angles of $\approx 40°$ and $\approx 70°$ [8], discontinuous changes in film thickness occur, corresponding to the last two layering transitions respectively. In the first part of this paper, we focus

on the frictional behavior of both the monolayers and the first additional bilayers [9]. In the second part, we use video microscopy to monitor the expulsion of the last thin layer of alcohol molecules between the surface bound monolayers. A two-dimensional hydrodynamic model is presented, which accounts for characteristic features of the expulsion process [10, 11].
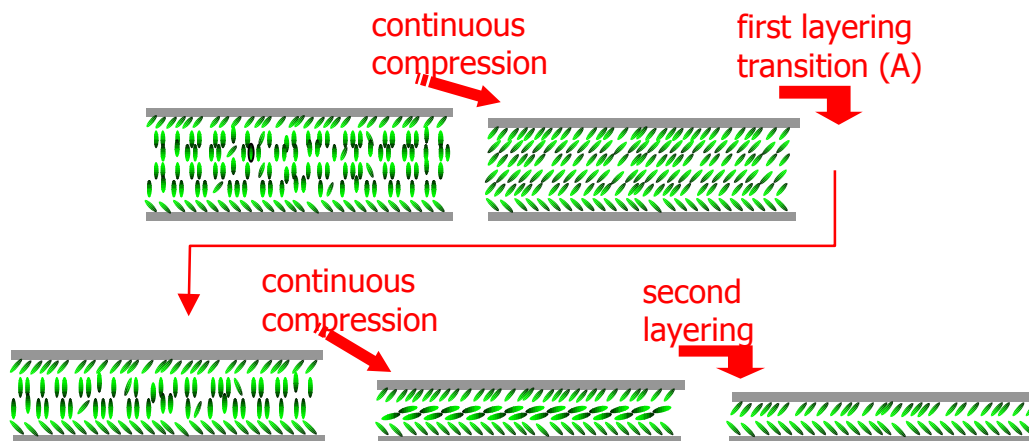

Fig. 1. Schematic representation of the structure of confined octanol films in various stages of compression and layering transitions.

Experiment

The surface forces apparatus that was used in this study was described in an earlier communication [7]. Briefly, the conventional FECO (fringes of equal chromatic order) technique is used to monitor the separation of the mica surfaces with a resolution of ± 2 Å. FECO fringes are recorded with a CCD camera and saved on a computer hard drive. The normal force is controlled by varying the current through magnetic coils that produce a magnetic field. The latter generates a force on a permanent magnet attached to the spring that holds the lower mica sheet. Reversing the coil current allows for very fast increase of the normal force ($\Delta F_n \approx 40$ mN within <100 ms). To measure friction forces, the upper mica surface is mounted on a stage, which can be laterally displaced using a piezo bimorph. A second piezo bimorph is used to sense the actual displacement [12]. The details of both setup and data analysis procedure were described previously [9].

The alcohols were purchased from Fluka (purity > 99.5%) and used as received. The experiments were performed at a room temperature of 22 ± 1°C. The mica surfaces were cleaved one more time immediately prior to the experiment, i.e. after gluing them to the cylindrical lenses and in particular after the hot wire melt cut

procedure [13]. This removes any possible contamination of the surfaces with particles that are typically created by the hot wire cutting [14]. The second cleavage is performed in a glove box under dry nitrogen atmosphere.

Results and Discussion

A. Friction and contact area

When the surface-bound monolayers are in direct contact, periodic stick-slip motion is observed upon shearing the surfaces, as shown in the inset of Fig. 2. The combined thickness of the monolayers on each mica surface is 23 Å. Both, the amplitude of the stick-slip motion and the absolute value of the friction force increase with load. Fig. 2 shows the maxima and minima of the stick-slip friction curves as a function of load, designated as critical and kinetic shear force, respectively. Two different models are typically used to analyze to load-dependence of friction forces. The first one is the classical Amontons law:

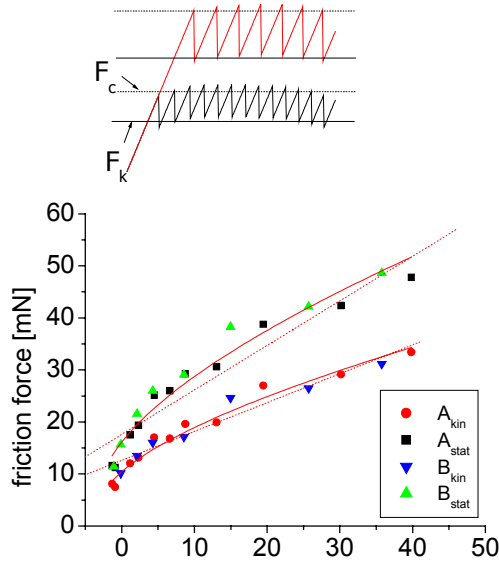$$F_{friction} = \mu \cdot F_N \qquad (1)$$

Fig. 2. Critical and kinetic friction force *vs.* load at a constant sliding speed of 1 μm/s for $C_{11}OH$. A and B correspond to independent experiments. Dotted lines are linear fits and solid lines are curves fitting the JKR model.Top: Shear force vs. time for stick-slip friction at two different loads.

where F_N is the load and μ is the static or the kinetic friction coefficient, which are both assumed to be independent of F_N. This law has been observed to hold for most macroscopic sliding surfaces. To be able to account for a finite friction force at zero external load, the friction force is usually augmented by a constant term F_0, which is proportional to the real area of contact at zero load. The physical origin of this term is related to adhesion between the surfaces. The dashed linear fits in Fig. 2 yield values for the static and kinetic friction coefficients of $\mu_{stat} = 0.89 \pm 0.07$ and $\mu_{kin} = 0.60 \pm 0.04$, respectively. (Errors indicate the statistical deviations from the fitting routine). The microscopic

justification of Amontons´ law is based on elastoplastic contact theory for surfaces with random roughness [15] or by the presence of contamination on the surfaces [16]. For clean single asperity contacts, the friction force should be proportional to the real area of contact.

$$F_{friction} = \sigma \cdot A(F_N) \qquad (2)$$

where σ is the critical or the kinetic shear stress, which are characteristic of the sliding materials and can depend on the contact pressure $F_N/A(F_N)$. (We prefer to designate the static friction force per unit contact area by "critical" instead of "static" shear stress.) $A(F_N)$ is the load-dependent contact area. For the crossed cylinders geometry of the SFA and surfaces with finite adhesion, the increase of the radius of

$$a^3 = \frac{R}{K}(F_N + 6\pi\, R\gamma + \sqrt{12\pi\, R\gamma F_N + (6\pi\, R\gamma)^2})$$

the contact area with load is assumed follow the Johnson, Kendall and Roberts (JKR) model [4]:

$$(3)$$

Here R ($\approx$ 2 cm) is the radius of curvature of the mica surfaces, K is the effective elastic modulus of the mica sheets and the underlying glue layers and γ is the interfacial energy of the substrate-liquid interface. Using (3) and assuming a perfectly circular contact, we obtain values of σ_c = 6.2 $\pm$ 0.9 MPa and σ_{kin} = 4.1 $\pm$ 0.7 MPa.
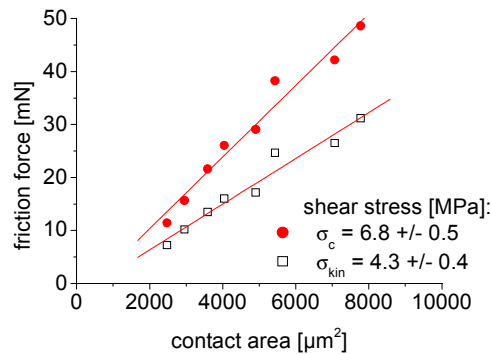

Fig. 3. Critical and kinetic friction force vs. the measured contact area (same friction data as in Fig.

Clearly, the solid lines in Fig. 2 fit the experimental data better than the dashed lines. The same result can also be obtained by plotting the friction force versus the contact area measured directly (Fig. 3). The diameter of the contact as a function of load was determined with an accuracy of $\pm$1 μm. This leads to an error in the contact area between 15% and 11% for the smallest and the highest

5

loads, respectively. The fits in Fig. 3 yield $\sigma_c = 6.8 \pm 0.5$ MPa and $\sigma_{kin} = 4.3 \pm 0.4$ MPa, which agree, within the statistical error, with the values obtained from the JKR fits.

B. Velocity dependence of shear stress

Next, we investigated the dependence of the critical shear stress on the (average) sliding speed in the stick-slip regime (Fig. 4). The critical shear stress is found to depend only weakly on sliding speed between 0.1 and 10 µm/s. At the high speed end a decrease is observed, whereas an increase appears at the lowest speeds. The former indicates that the transition to continuous sliding would have been reached at only slightly higher sliding speeds. Unfortunately however, these speeds were not accessible in the present experiments.
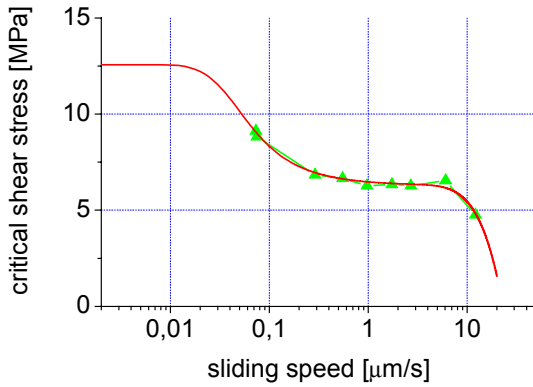

Fig. 4. Critical shear stress vs. sliding speed at $F_N = 8.8$ mN. The solid line is a fit according to eq. (5) in the text, which describes the exponential growth of inter-digitation or, in our case crystallographicaly locked domains.

The observed speed dependence can be rationalized with the following picture of the sliding process: During the stick phase the monolayers on the opposing mica surfaces can relax and increase their mutual interlocking or crystallographic matching, starting at several nucleation points. The growth of such locked domains can be described by an exponential law with characteristic time τ. The critical shear stress thus relaxes exponentially with sticking time t_{stick} and reaches its maximal value only for $t_{stick} \gg \tau$ [17]

$$\sigma_c(t_{stick}) = \sigma_{c,0} + \Delta\sigma \cdot (1 - \exp(-t_{stick}/\tau)) \qquad (4)$$

Here $\sigma_{c,0}$ is the initial critical shear stress before relaxation, and $\Delta\sigma$ is the difference between σ_c ($t_{stick}=\infty$) and $\sigma_{c,0}$. The speed dependence of the critical shear stress thus reflects the relation between the relaxation time τ and the average sticking time $\langle t_{stick} \rangle$, which decreases as the average sliding speed is increased. To model our data, we had to assume the presence of two different relaxation processes, which were given equal weight.

$$\sigma_c(t_{stick}) = \sigma_{c,0} + \Delta\sigma \cdot (1 - 0.5 \cdot \exp(-t_{stick}/\tau_1) - 0.5 \cdot \exp(-t_{stick}/\tau_2)) \qquad (5)$$

The solid line in Fig. 4 is a fit to the data with τ_1=0.36 s, τ_2= 280 s, and σ_c (t_{stick}=∞) = 12.6 MPa. ($\sigma_{c,0}$ was set to zero).

Eq. (4) was originally introduced to model the increase in critical shear stress with time due to interdigitation of molecules in opposing surface-bound layers. Alternatively, cooperative motion of a large number of molecules could also explain the observations. Since the monolayers are likely to consist of large number of domains of closely packed alkyl chains [7, 9], collective relaxation of both polar or azimuthal angle of the molecules within the domains could give rise to a slow relaxation time. Relaxation of the average polar angle under pressure and shear was observed in AFM experiments with self-assembled monolayers of both various alkyl-silanes on mica [18] and alkyl-thiols on gold [19]. Although in these experiments the applied pressure was two to three orders of magnitude higher, the alcohol molecules are much more mobile and more weakly bound to the substrate [20], which may allow for similar processes to occur at much lower pressures. The compactness and the size distribution of the domains could also be modified during the sliding process. These "annealing processes" would restore the original structure during the stick phase. Annealing processes and ripening have been observed in SAMs of thiols and silanes with time scales of hours to days [21]. Again, the higher mobility for the alcohol molecules could bring the time scale down to the observed range of τ_2.
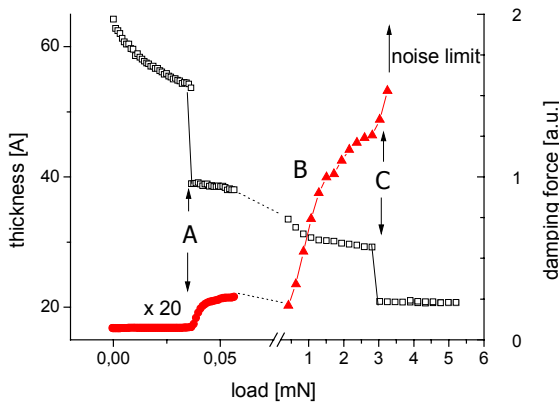
C. Rheological measurements

Fig. 5. Damping force (triangles) and film thickness (squares) for octanol subjected to shear between mica surfaces *vs.* applied load. The damping force is proportional to the viscosity. Symbols A, B and C indicate the corresponding states in Fig. 1. In region B the separation between mica surfaces remains constant but the area of the contact increases. The damping force at low loads is shown magnified 20 times. Notice the change in the load scale in region B.

At larger surface separation the stick-slip motion was never observed. This was true even with a single additional liquid (bi)layer between the surface-bound monolayers. To study the lubrication properties of such thin films, we performed rheological experiments, where the mica surfaces were sheared laterally with an

7

amplitude of 2 nm at a frequency of 10 Hz [9]. Fig. 5 shows the damping due to the alcohol layer as well as the film thickness as the load was increased. Note the break in the load axis and the magnification of the damping curve at small loads. The loads corresponding to the last two layering transitions are marked A and C, as in Fig. 1. Region B is corresponds to the continuous compression of the last bilayer trapped between the fixed monolayers. The most important aspect of this curve is that it shows that only a very small increase in damping occurs at the layering transition A. The subsequent increase during phase B essentially reflects the increase in contact area. Together with the absence of stick-slip it indicates that the additional material between the fixed monolayers behaves like a liquid, with a viscosity close to its bulk value. This result is very different from other substances (OMCTS, cyclohexane, linear alkanes), where large increases in viscosity due to solidification were observed at film thickness between 4 and 6 layers [5, 6]. We attribute this difference to the specific structure of the alcohol films. The surface-bound monolayers shield the lateral potential corrugation of the mica and provide a smooth CH_3-terminated surface for the additional liquid. A similar role of the surface bound layers was observed in molecular dynamics simulations of linear alkane molecules when the molecule-substrate interaction was increased [22].

D. Dynamics of Layering Transition

The dynamics of liquid expulsion in two dimensions was studied by imaging the contact. To that end we modified our experimental set-up slightly [10]. Instead of using white light, we illuminated the contact area with monochromatic light. The wavelength was chosen near the edge of the transmission peak of the Fabry-Perot interferometer formed by the silver mirrors in the backsides of the mica, with the surfaces in contact. In this case the intensity of the transmitted light changes rapidly with changes in the thickness of the gap in the nanometer range. Images of the intensity variations accross the contact were acquired and stored on video tape. The experiments were performed as follows. Starting at a surface separation of several micrometers, the normal force was abruptly increased from 0 to 20 mN. As a result, the surfaces approached each other with an initial speed >100 μm/s and most of the liquid between them were expelled. From conventional SFA experiments at low approach speeds, we know that at this load the substrate-bound monolayers come into

direct contact under equilibrium conditions. However, in the present experiments some liquid remains trapped between the surfaces in a metastable state. Within <0.2 sec, the apex of the two curved surfaces (initial radius of curvature ≈ 2 cm) flatten out and form a flat contact area with a radius of 40 μm. This corresponds to an

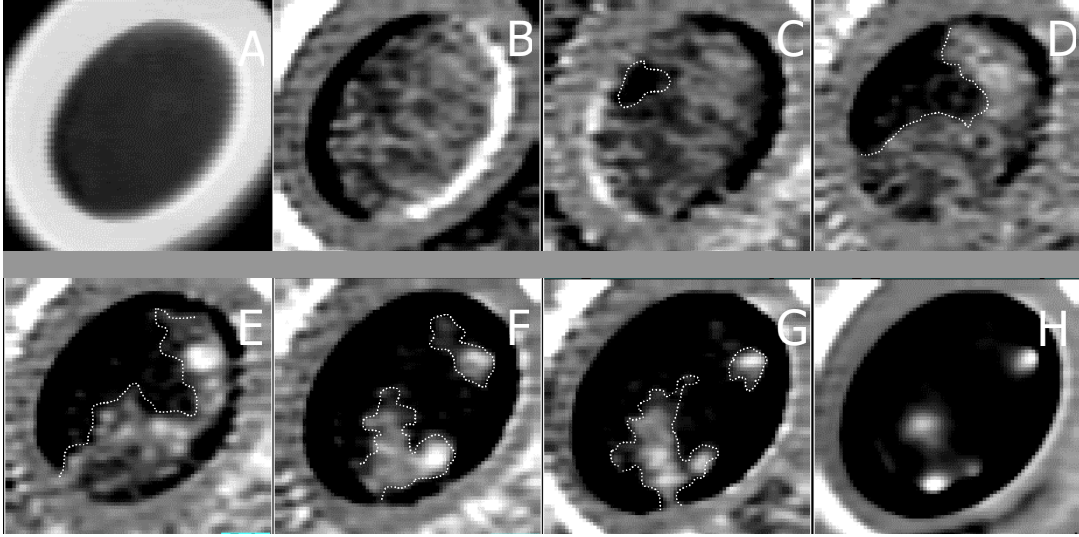Fig. 6. Snapshots of the contact area during the layering transition (100 μm × 100 μm size). The initial (A) and final state (H) images are averaged for noise reduction. Images B to H are difference images with the initial state (A). Images B to G are recorded at 0.16 sec time intervals. Darker color corresponds to smaller film thickness. The dark and bright rim at the edge of the contact area in B and C are artifacts related to the subtracting of video images.

average pressure of ≈ 4 MPa. The intensity across the contact area is homogeneous and stays constant for a certain time (Fig. 6A and B). After typically less than 20 s, a darker area corresponding to a region of reduced film thickness opens up inside the contact (Fig. 6C). This nucleus grows and spreads across the whole contact area within < 1s (D to G). During the growth process, the boundary line delimiting the drained region bends in a double S-shaped fashion (D, E) and becomes rough. As the roughness increases, pockets containing non-expelled material detach from the boundary line (F, G) and are left behind trapped inside the contact area in the final state (H). Note that some of the pockets in (H) are brighter (i.e. thicker) than the initial metastable layer in (B). Most of the trapped pockets remain for at least several minutes. Others that are located close to the edges of the contact area eventually get squeezed out.

In principle, it is possible to calculate the thickness of the trapped film from the transmitted intensity. Unfortunately, calibration problems with the absolute intensity prevented this for the present set of data [23]. Therefore we do not know the exact thickness of the pockets under the non-equilibrium conditions of the present experiment. The same uncertainty applies to the thickness of the initially trapped

metastable layer. However, since the final state patterns and the typical times for the expulsion process were the same in both the fast squeeze experiments and in the conventional slower force-distance measurements, we conclude that the thickness of the expelled layer is also the same in both experiments.

The various aspects of the dynamics in Fig. 6 can be understood on the basis of a two-dimensional hydrodynamic model [10, 11, 24, 25]. In the simplest approximation the dynamics of the layering transition is described by a two-dimensional potential flow of an incompressible liquid [24]. This means that the full two-dimensional Navier Stokes equation is replaced by the Laplace equation:

$$\nabla^2 \Phi = 0 \qquad (6)$$

The flow potential is given by $\Phi = -P_{2D}/(\rho\eta)$ and the liquid velocity is $v = \nabla\Phi$. P_{2D} is the two-dimensional pressure, ρ the density of the fluid and η the friction coefficient of the sliding liquid layer on the substrate. The major driving force for the transition, i.e. the dominant contribution to P_{2D}, is provided by the applied load that deforms the mica substrates elastically. When a hole in the metastable layer opens up, elastic strain energy is gained by relaxing the mica locally. This translates into a two-dimensional pressure P_{2D}. The motion of the boundary line is opposed by the friction of the molecules being expelled against the surface. Along the boundary of the (initially circular) nucleus P_{2D} decreases with distance from the center of the contact area according to the Hertzian expression. At the edge of the contact area it is constant. Therefore, the pressure gradient is the largest where the boundary is closest to the edge (Fig. 7a). As a result any nucleus that appears off-center initially will grow asymmetrically and reach the closest edge of the contact first. Solving eq. (6) numerically, we showed [24] that this indeed leads to the double-S-shaped boundary we observed in Fig. 6 D and E.
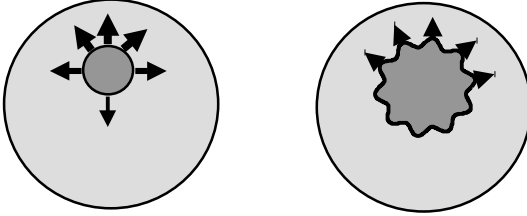
Fig. 7. a) Schematic of an off-center hole (dark area). The two-dimensional pressure gradient between the boundary of the hole and the edge of the contact is steepest where their separation is minimal, leading to a larger flow velocity, as indicated by the arrows. b) Same situation as in a), for a hole with a perturbed boundary. Arrows indicate how the differences in pressure gradient let the perturbation increase with time.

The same argument can be used to explain the subsequent roughening of the boundary line [25]. Fig. 7b shows a sketch of a hole with a deformed edge. The boundary line is closer to the edge of the contact area at the peaks of the disturbance than at the valleys. Hence the amplitude of the disturbance is expected to increase with time and lead to an indefinite roughening of the boundary line. This does not occur if a line tension is taken into account, since this will tend to straighten the boundary line. There are two contributions to the line tension in this system. The first one is a "broken bond" contribution due to the lack of neighbors for the molecules along the boundary line. The second one is due to the difference in elastic strain inside the mica in the vicinity of the boundary line. For all practical purposes, the latter is two to three orders of magnitude larger than the former. Using linear instability analysis, we have shown that for typical line tension values derived from surface tensions of alkane hydrocarbons, there is a critical wavelength $\lambda_c \approx 5$ μm below which the contact line is expected to be smooth [25]. This value is in reasonable agreement
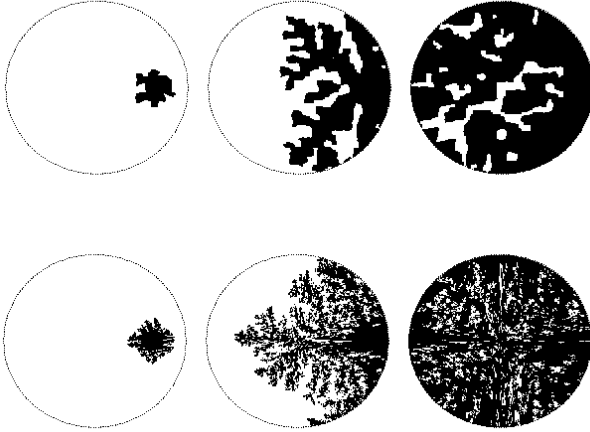

Fig. 8. Snapshot of the layering transition in the kinetic Monte Carlo simulation. Top: with and bottom: without line tension. To calculate the P_{2D}, a radial pressure distribution according to Hertzian contact theory was used.

with the experimentally observed roughness in Fig. 6. If line tension is neglected, the expulsion pattern looks very different, as shown recently using kinetic Monte Carlo simulations [11]. In that case, the boundary line roughens and becomes fractal on all length scales down the grid size of the simulation (Fig. 8b). Only when a finite value of line tension is used, the simulated shape of the

boundary agrees with the experimental observation (Fig. 8a). It is still fractal, but now only on length scales above a certain smoothing length, which is on the order of λ_c for the correct value of line tension.

E. Trapped pockets

The success of the hydrodynamic model corroborates that the material that is expelled is indeed in a liquid-like state, as we found in the rheological measurements

discussed above. Nevertheless, being purely two-dimensional the model should fail to describe the observed increase in the thickness of the trapped pockets. The latter can be explained under quasi-static conditions by simply considering the total energy of a fixed amount of liquid trapped inside the contact area [10]. Briefly, there is first a contribution from the interfacial energy between the substrate (including the surface-bound monolayers) and the liquid layer. A second one arises from the line tension along the boundary line, as discussed above. The trapped liquid can reduce the interfacial energy by shrinking laterally. Because of the fixed volume constraint, it has to deform the mica elastically simultaneously. The balance of the two contributions leads to the energetically most favorable shape. The resulting values for the thickness of the pockets [10] are in agreement with the experimentally observed ones. A detailed comparison, however, has to await more accurate measurements. It is interesting to note that local transformations to larger thickness do also occur transiently during the expulsion process (see the brighter gray levels in Fig. 6E and F). This coupling of two-dimensional liquid expulsion to three dimensional substrate deformations is clearly missing in the present description of the dynamics and should be more pronounced the softer the substrates are. In this context it is important to note that in the present experiment the total thickness of the mica substrates was only <300 nm, which makes the effective substrate (mica plus underlying glue) rather soft. Even more pronounced substrate deformations were observed by Martin and Brochart [26] when they investigated the dewetting of silicone oil films between silicon and a soft rubber surface. In terms of the importance of substrate elasticity, our experiments represent an intermediate case between those experiments and most other SFA experiments where mica sheets are typically a few micrometers thick.

Conclusion

Chain alcohols were shown to have unique lubrication properties in a surface forces apparatus. Their strong interaction with the substrate leads to an effective decoupling of the surface-bound monolayers from the rest of the liquid inside the gap. Owing to the weak coupling, slip occurs easily at the interface between the monolayers and the additional liquid. Therefore the alcohol films do not sustain any shear stress, as long as there is a single layer of liquid separating the surface-bound monolayers. Only when they come into direct contact the monolayers display solid-like stick-slip friction with a critical shear stress of σ_c =6.2 MPa.

Being in a liquid state, the last layer of alcohol molecules could be expelled from the gap quickly under external pressure. Two-dimensional imaging of the expulsion process revealed a rich dynamic behavior. The interplay between elastic relaxation, which drives the transition, and friction forces, which oppose the motion of the liquid layer, leads to growth instabilities. The boundary line between the areas of final and initial film thickness bends and roughens in a characteristic way. Most aspects of the process are successfully described in terms of a two-dimensional hydrodynamic model. Kinetic Monte Carlo simulations show that the roughening can only be properly explained when the line tension of the boundary line is taken into account. Interestingly, deviations from the purely two-dimensional behavior in the form of thickening pockets of trapped liquid appear due to the finite elasticity of the substrates. This new aspect of squeezing dynamics deserves further attention in future studies.

References

[1] D. S. Greywall and P. A. Busch, Phys. Rev. Lett. **67**, 3535 (1991).

[2] F. Mugele, U. Albrecht and P. Leiderer, J. Low Temp. Phys. **96**, 177 (1994); D. Cieslikowski, A. Dahm, and P. Leiderer, Phys. Rev. Lett. **58**, 1751 (1987).

[3] O. M. Magnussen, B. M. Ocko, M. J. Regan, K. Penanen, P. S. Pershan, and M. Deutsch, Phys. Rev. Lett. **74**, 4444 (1995).

[4] J.N. Israelachvili, *Intermolecular and Surface Forces* (Academic Press, London, UK, 1985).

[5] J. Klein and E. Kumacheva, Science **269**, 816 (1995); J. Klein and E. Kumacheva, J. Chem. Phys. **108**, 6996 (1998); E. Kumacheva and J. Klein, J. Chem. Phys. **108**, 7010 (1998).

[6] M. L. Gee, P. M. McGuiggan, J. N. Israelachvili, and A. M. Homola, J. Chem. Phys. **93**, 1895 (1990); H. Yoshizawa and J. N. Israelachvili, J. Phys. Chem. **97**, 11300 (1993).

[7] F. Mugele and M. Salmeron, J. Phys. Chem. B **104**, 3140 (2000).

[8] The numbers refer to C_8OH. In the case of $C_{11}OH$, different molecular arrangements seem to compete. See [7] for a detailed discussion.

[9] F. Mugele and M. Salmeron, J. Chem. Phys. **114**, 1831 (2001).

[10] F. Mugele and M. Salmeron, Phys. Rev. Lett. **84**, 5796 (2000).

[11] S. Zilberman, B. N. J. Persson, A. Nitzan, F. Mugele, and M. Salmeron, Phys. Rev. E **63**, available electronically.

[12] J. Peachey, J. van Alsten , and S. Granick, Rev. Sci. Instrum. **62**, 463 (1991).

[13] P. Frantz and M. Salmeron, Tribol. Lett. **5**, 151 (1998).

[14] S. Ohnishi, M. Hato, K. Tamada, and H.K. Christenson, Langmuir **15**, 3312 (1999).

[15] F. P. Bowden and D. Tabor, *The friction and Lubrication of Solids* (Clarendon Press, Oxford, 1986).

[16] G. He, M.H. Müser, and M.O. Robbins, Science **284**, 1650 (1999).

[17] B. N. J. Persson, *Sliding Friction* (Springer Verlag, New York, 1998), Chapt. 12.

[18] E. Barrena, S. Kopta, D.F. Ogletree, D.H. Charych, and M. Salmeron, Phys. Rev. Lett. **82**, 2880 (1999).

[19] E. Barrena, C. Ocal, and M. Salmeron, J. Chem. Phys. **113**, 2413 (2000).

[20] In contrast to silanes on mica, islands of alcohol molecules with identical alkyl chain length (C_{16}) cannot be imaged by contact mode AFM (F.M., unpublished data).

[21] E. Barrena, C. Ocal and M. Salmeron, J. Chem. Phys. **111**, 9797 (1999).

[22] E. Manias, G. Hadziioannou, and G. ten Brinke, Langmuir **12**, 4587 (1996); E. Manias, I. Bitsanis, G. Hadziioannou, and G. ten Brinke, Europhys. Lett. **33**, 371 (1996).

[23] Experiments to resolve the remaining uncertainty are under way.

[24] B. N. J. Persson and E. Tosatti, Phys. Rev. B **50**, 5590 (1994).

[25] B. N. J. Persson, Chem. Phys. Lett. **324**, 231 (2000).

[26] P. Martin and F. Brochard-Wyart, Phys. Rev. Lett. **80**, 3296 (1998).